

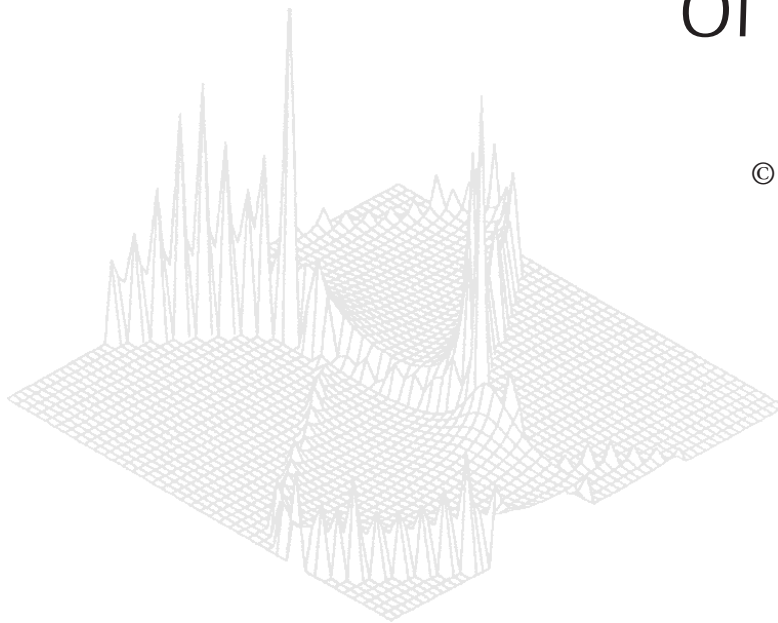
---

CSIRO PUBLISHING

---

# Australian Journal of Physics

Volume 52, 1999  
© CSIRO Australia 1999



A journal for the publication of  
original research in all branches of physics

[www.publish.csiro.au/journals/ajp](http://www.publish.csiro.au/journals/ajp)

All enquiries and manuscripts should be directed to

*Australian Journal of Physics*

**CSIRO PUBLISHING**

PO Box 1139 (150 Oxford St)

Collingwood

Vic. 3066

Australia

Telephone: 61 3 9662 7626

Facsimile: 61 3 9662 7611

Email: [peter.robertson@publish.csiro.au](mailto:peter.robertson@publish.csiro.au)



Published by **CSIRO PUBLISHING**  
for CSIRO Australia and  
the Australian Academy of Science



## Ordered and Disordered Photonic Band Gap Materials\*

R. C. McPhedran,<sup>A</sup> L. C. Botten,<sup>B</sup> A. A. Asatryan,<sup>A</sup> N. A. Nicorovici,<sup>A</sup>  
C. Martijn de Sterke<sup>A</sup> and P. A. Robinson<sup>A</sup>

<sup>A</sup>School of Physics, University of Sydney, NSW 2006, Australia.

<sup>B</sup>School of Mathematical Sciences, University of Technology,  
Sydney, NSW 2007, Australia.

### *Abstract*

We discuss a formulation and computer implementation of a new method that can be used to determine the electromagnetic properties of ordered and disordered dielectric and metallic cylinders, using periodic boundary conditions in one direction. We show results which exhibit strong parallels with the behaviour of electrons in disordered semiconductors, but also illustrate some characteristics which clearly differentiate between photonic and electronic behaviour. Among these are strong polarisation sensitivity and effects due to metallic absorption.

### 1. Introduction

There is much current work in the theory and applications of photonic band gap materials, whose development is based on an attempt to parallel that of semiconductors in the 1960s and 1970s. The aim (Soukoulis 1993; Joannopoulos *et al.* 1995) is to construct materials in which there is a band gap for photons, so that only evanescent waves are allowed for well-defined ranges of photon energy, irrespective of the photon's direction of propagation and polarisation. As one measure of the interest in this field, the latest release of the online bibliography of the field (Dowling *et al.* 1998) contains 685 references from the last ten years.

As well as constructing materials with band gaps for photons, a natural next requirement would be to alter the structure in such a way as to produce the equivalent of impurity states inside the optical band gap. One structure of current interest, and which has the potential to fulfil these goals, consists of stacks of layers of dielectric cylinders. As long as the refractive index of the cylinders is sufficiently large (say 3 or greater), then a few layers of cylinders can be sufficient to develop a clear in-plane band gap. Variation of the refractive index of one or more cylinders causes the appearance of the equivalent of impurity levels inside the gap (Soukoulis 1993; Joannopoulos *et al.* 1995).

We have developed a new formulation capable of analysing the optical behaviour of stacks of cylinders with unprecedented speed and resolution. This formulation is based on pioneering work of von Ignatowsky (1914) and Twersky (1961). However,

\* Refereed paper based on a contribution to the Eighth Gordon Godfrey Workshop on Condensed Matter Physics held at the University of New South Wales, Sydney, in November 1998.

it represents a considerable generalisation of their purely analytic work, in that a numerical implementation is developed which treats grating layers having an arbitrary number of different cylinders in each period, rather than just one cylinder per period. Furthermore, an arbitrary number of grating layers can be stacked one behind the other, with the resultant behaviour being evaluated using a powerful matrix recurrence technique. The resulting formulation has some similarities with those in previous work (Wijngaard 1973; Felbacq *et al.* 1994; Lo *et al.* 1994; Li and Zhang 1998), chiefly in its use of Graf's addition theorem (Abramowitz and Stegun 1972), but differs from previous work in its combination of periodic boundary conditions within each layer, and the use of recurrence relations to couple the layers. Our new method is capable of delivering results of high accuracy for quite large systems using modest computer resources (workstations, or clusters of workstations). It is also distinguished by its ability to handle cylinders of complex refractive index with large modulus, unlike techniques based on finite differences or plane wave expansions (Ho *et al.* 1990; Leung and Liu 1990; Pendry and MacKinnon 1992).

Here, we report on some of the first results of this formulation, exhibiting both parallels with and differences from the behaviour of electrons in semiconductors. Important differences which we highlight between photons and electrons arise because of the natural roles of polarisation and absorptance for photons.

## 2. Formulation

We model the propagation of electromagnetic waves through the structure shown in Fig. 1. This is a stack of gratings, each of which consists of a singly periodic set of parallel cylinders of different radii, with the centres located on the  $x$ -axis. In each grating there is an element (the 'unit cell' of the grating, in our case of length  $D$ ) which is repeated along the  $x$ -direction, thus making the grating periodic. The cylinders inside the unit cell of the grating may have random  $x$ -positions, random radii and random refractive indices. For the stack of gratings we may add two other random elements; the characteristics of the cylinders inside the unit cells of different gratings, and the distance between successive gratings. Each of the gratings has been taken to have a common period  $D$ , so that the grating stack may be regarded as a composite grating with this period. We assume that the medium between cylinders is a vacuum.

### (2a) The Rayleigh Identity

We consider only the problem with the incident radiation in the  $xy$  plane, characterised by the wave vector

$$\mathbf{k} = (\alpha_0, \chi_0, 0), \quad (1)$$

with

$$\alpha_0 = k \sin \theta_0, \quad \chi_0 = k \cos \theta_0. \quad (2)$$

Here,  $k = 2\pi/\lambda$ ,  $\lambda$  is the wavelength of the radiation in vacuo, and  $\theta_0$  is the angle of incidence with respect to the  $y$ -axis.

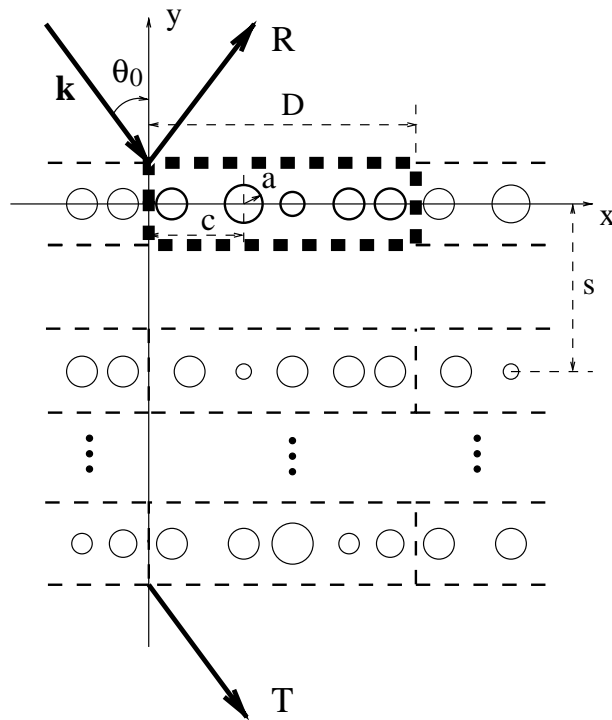


**Fig. 1.** Schematic of the structure we consider. It consists of gratings with cylinders of random radii ( $a$ ) and random positions ( $c$ ). The unit cell in the first grating is marked by the thick dashed line. We also show the incident, reflected and transmitted waves corresponding to the zeroth order of diffraction.

We begin by considering a single grating. Above and below the grating the fields are expressed as plane wave expansions (McPhedran *et al.* 1997a):

$$V(x, y) = \sum_{p=-\infty}^{\infty} \chi_p^{-1/2} (\delta_{p0} e^{-i\chi_0 y} + \rho_{p0} e^{i\chi_p y}) e^{i\alpha_p x}, \quad (3)$$

above the grating ( $y > 0$ ), and

$$V(x, y) = \sum_{p=-\infty}^{\infty} \chi_p^{-1/2} \tau_{p0} e^{i(\alpha_p x - \chi_p y)}, \quad (4)$$

below the grating ( $y < 0$ ). Here,  $\rho_{p0}$  and  $\tau_{p0}$  represent the amplitude reflection and transmission coefficients for the  $p^{\text{th}}$  diffraction order with an incident wave from above in the order  $p = 0$ , and

$$\alpha_p = \alpha_0 + p \frac{2\pi}{D}, \quad \sin \theta_p = \alpha_p / k. \quad (5)$$

$$\chi_p = \begin{cases} \sqrt{k^2 - \alpha_p^2} & \text{if } p \in \Omega \equiv \{p \mid \alpha_p^2 < k^2\}, \\ i\sqrt{\alpha_p^2 - k^2} & \text{if } p \in \bar{\Omega} \equiv \{p \mid \alpha_p^2 > k^2\}. \end{cases} \quad (6)$$

Note that equations (5) and (6) define the propagating orders, corresponding to  $p \in \Omega$ , and evanescent orders, corresponding to  $p \in \bar{\Omega}$ . The term  $\chi_p^{-1/2}$  in (3) and (4) is included to simplify energy calculations, yielding normalised expressions for diffraction efficiencies that are simply the square moduli of the corresponding amplitudes.

In the vicinity of the grating, we express the fields in the natural basis functions for cylinders [cylindrical harmonics (Abramowitz and Stegun 1972) labeled by  $m$ ] and exploit a representation of the Green function in this basis (Nicorovici and McPhedran 1994; McPhedran *et al.* 1997a):

$$G(r, \theta) = \frac{1}{4i} \left[ H_0^{(1)}(kr) + \sum_{m=-\infty}^{\infty} S_m J_m(kr) e^{im\theta} \right]. \quad (7)$$

In (7), the  $S_m$  denote the lattice sums (Nicorovici and McPhedran 1994; McPhedran *et al.* 1997a):

$$S_m = \sum_{n \neq 0} H_m^{(1)}(|n|kD) e^{im\theta_n} e^{i\alpha_0 n D}, \quad (8)$$

where  $\theta_n = \pi H(-n)$ , with  $H(n)$  denoting the Heaviside function. The evaluation of the  $S_n$  was considered analytically by von Ignatowsky (1914) for normal incidence, and Twersky (1961) developed convenient expressions for accurate evaluation of the  $S_n$  in the general case of oblique incidence.

Now the scattering of polarised electromagnetic waves by a grating is solved in terms of a single Cartesian component  $V$  of the electric field  $\mathbf{E}$  or magnetic field  $\mathbf{H}$  which, in the neighbourhood of a particular cylinder, is written as

$$V(r, \theta) = \sum_{m=-\infty}^{\infty} [A_m J_m(kr) + B_m Y_m(kr)] e^{im\theta}. \quad (9)$$

We can apply the boundary conditions at the cylinder surface, to give (McPhedran *et al.* 1997b)

$$A_m = -M_m B_m, \quad (10)$$

where the  $M_m$  are analytically known and depend on the polarisation. For example, for  $E_z$  polarisation ( $V = E_z$ ) the  $M_m$  coefficient takes the form (McPhedran *et al.* 1997b)

$$M_m = \frac{nJ'_m(nka)Y_m(ka) - J_m(nka)Y'_m(ka)}{nJ'_m(nka)J_m(ka) - J_m(nka)J'_m(ka)}, \quad (11)$$

where  $a$  is the radius of the cylinder and  $n$  is its refractive index.

The  $B_m$  coefficients are determined for each cylinder in the period cell using a Rayleigh identity (McPhedran *et al.* 1997a) which expresses the part of  $V$  which is regular at the origin in terms of sources on all the other cylinders in the grating, plus sources at infinity. In our case, when we have more than one cylinder inside the unit cell, the Rayleigh identity (associated with cylinder  $l$ ) becomes

$$iM_n^l B_n^l + \sum_{q=1}^{N_c} \sum_{m=-\infty}^{\infty} S_{n-m}^{lq} B_m^q = -i(-1)^n e^{i\alpha_0 c_l} e^{-in\theta_0} \chi_0^{-1/2}. \quad (12)$$

Here,  $l$  and  $q$  are labels for the cylinders inside the unit cell,  $N_c \geq 1$  represents the total number of cylinders in the unit cell, and  $c_l$  is the coordinate of the centre of cylinder  $l$  (see Fig. 1). The right-hand side of (12) derives from the cylindrical harmonic components of the incident field, representing wave sources at infinity. Below we generalise this incident field to include all possible plane wave components necessary to describe completely general incident fields, as is required for the filling of scattering matrices.

In (12), the  $S_m^{lq}$  are lattice sums for the local environment of each cylinder, which have been used to reduce the sums over cylinders to just those lying in the central unit cell. They can be obtained from global lattice sums  $S_m$  using Graf's addition theorem. Thus, for  $l = q$  we obtain

$$S_m^{ll} = S_m + \delta_{m0}, \quad (13)$$

where  $\delta$  is the Kronecker symbol while, for  $l \neq q$ , we have

$$S_m^{lq} = iY_m(k|c_q - c_l|)e^{im\theta_{lq}} + \sum_{n=-\infty}^{\infty} S_{m+n} J_n(k|c_q - c_l|)e^{in(\pi - \theta_{lq})}, \quad (14)$$

with  $\theta_{lq} = \pi H(c_l - c_q)$ .

In terms of  $B$  coefficients the amplitude reflection and transmission coefficients for incidence in order 0 are

$$\rho_{p0} = \frac{2}{iD} \chi_p^{-1/2} \sum_{m=-\infty}^{\infty} e^{-im\theta_p} \sum_{l=1}^{N_c} B_m^l e^{-i\alpha_p c_l}, \quad (15)$$

$$\tau_{p0} = \delta_{p0} + \frac{2}{iD} \chi_p^{-1/2} \sum_{m=-\infty}^{\infty} (-1)^m e^{im\theta_p} \sum_{l=1}^{N_c} B_m^l e^{-i\alpha_p c_l}. \quad (16)$$

### (2b) Scattering Matrices

We solve the Rayleigh identity (12) to obtain the plane wave scattering matrix  $\mathcal{S}$ , which gives the output amplitudes in the various diffraction orders as the input ranges over all orders. The scattering matrices allow us to 'couple' the different gratings together to form a stack. We begin by considering the symmetric and

antisymmetric problems — the decomposition relying on the up–down symmetry in each grating layer, an assumption which is satisfied in the cases studied in this paper. The relations between the  $B$  coefficients in the Rayleigh identity and the multipole coefficients for the symmetric ( $\oplus$ ) and antisymmetric ( $\ominus$ ) problems are

$$C_n^{\oplus,\ell} = A_n^\ell + (-1)^n A_{-n}^\ell, \quad C_n^{\ominus,\ell} = A_n^\ell - (-1)^n A_{-n}^\ell, \quad (17)$$

$$D_n^{\oplus,\ell} = B_n^\ell + (-1)^n B_{-n}^\ell, \quad D_n^{\ominus,\ell} = B_n^\ell - (-1)^n B_{-n}^\ell, \quad (18)$$

$$C_n^{\oplus,\ell} = -M_n^\ell D_n^{\oplus,\ell}, \quad C_n^{\ominus,\ell} = -M_n^\ell D_n^{\ominus,\ell}, \quad (19)$$

for each cylinder  $\ell$  inside the unit cell and with  $n \geq 0$ . The use of the  $C$  and  $D$  coefficients means that we have ‘folded’ the Rayleigh identity (12), eliminating any reference to negative indices  $n$  and thus halving the dimension of the system of equations and set unknowns.

Before continuing we introduce some nomenclature conventions. We denote by  $\mathcal{M} = [\mathcal{M}_{ab}]$  a matrix of elements  $\mathcal{M}_{ab}$ . Similarly, the matrix  $\mathcal{M} = [\mathcal{M}^{cd}]$  denotes a *partitioned* matrix, the elements of which are matrices themselves. An example of this is the matrix  $\sigma^\oplus$ , defined in (24) below. Note that the number of dummy indices gives the rank of the resulting matrix. Thus a single index results in a vector; the vector is partitioned if its elements are vectors or matrices themselves. Examples of such vectors are  $\mathbf{J}^\oplus$ , defined in (26), and  $\mathbf{D}^\oplus$ , defined in the paragraph below.

To solve the symmetric problem we rewrite the Rayleigh identity (12) in terms of the single, unknown partitioned vector  $\mathbf{D}^\oplus$ , using (19) to eliminate the multipole coefficients  $\mathbf{C}^\oplus$ . Here  $\mathbf{D}^\oplus = [D_n^{\oplus,\ell}]$  is a block partitioned vector whose first block contains the multipole coefficients for cylinder 1, whose second block contains the coefficients for cylinder 2 and so on. We also introduce the block diagonal matrix  $\mathbf{M}$ , comprising the boundary condition quantities  $M_n^\ell$  from (10) and (19), with the Neumann symbol

$$\varepsilon_n = \begin{cases} \frac{1}{2} & \text{if } n = 0, \\ 1 & \text{if } n > 0 \end{cases} \quad (20)$$

accounting for the folding of the positive and negative multipole orders  $n$ . Here, we have

$$\mathbf{M} = \text{diag}[\mathbf{M}^\ell \boldsymbol{\varepsilon}^{-1}], \quad (21)$$

where

$$\mathbf{M}^\ell = \text{diag}[M_n^\ell], \quad \boldsymbol{\varepsilon} = \text{diag}[\varepsilon_n] \quad (22)$$

and where the  $M_n^\ell$  were defined in (19). We also require a diagonal matrix  $\chi$  defined as

$$\chi = \text{diag}[\chi_p], \quad (23)$$

consisting of direction cosines along the diagonal. The lattice sums for the symmetric problem comprise a square partitioned matrix  $\boldsymbol{\sigma}^\oplus$ , which is defined through

$$\boldsymbol{\sigma}^\oplus = [\boldsymbol{\sigma}^{\oplus, \ell q}], \quad \boldsymbol{\sigma}^{\oplus, \ell q} = [\boldsymbol{\sigma}_{nm}^{\oplus, \ell q}], \quad (24)$$

where the elements are linear combinations of lattice sums (14)

$$\boldsymbol{\sigma}_{nm}^{\oplus, \ell q} = S_{n-m}^{\ell q} + (-1)^n S_{n+m}^{\ell q}, \quad (25)$$

with block indices  $l$  and  $q$ , and with array indices  $n$  and  $m$ . Finally, we need a partitioned column vector  $\mathbf{J}^\oplus$ ,

$$\mathbf{J}^\oplus = [\mathbf{J}^{\oplus, \ell}], \quad \mathbf{J}^{\oplus, \ell} = [\mathbf{J}_{np}^{\oplus, \ell}], \quad (26)$$

where the elements of  $\mathbf{J}^{\oplus, \ell}$  are defined through

$$\mathbf{J}_{np}^{\oplus, \ell} = [e^{in\theta_p} + (-1)^n e^{-in\theta_p}] e^{i\alpha_p c_\ell}, \quad (27)$$

with block indices  $n$  for multipoles, and  $p$  for plane waves. The elements of  $\mathbf{J}^{\oplus, \ell}$  characterise coefficients of plane waves in expansions in cylindrical harmonics. In this way,  $\mathbf{J}^{\oplus, \ell}$  is the matrix representation of a change of basis from plane waves, which are used to describe the field away from the cylinders, to cylindrical harmonics, which are used to describe the field between cylinders.

Using the notation developed above, Rayleigh's identity (12) takes the simple form

$$(\boldsymbol{\sigma}^\oplus + i\mathbf{M}) \mathbf{D}^\oplus = -i\mathbf{J}^\oplus \chi^{-1/2} \boldsymbol{\delta}, \quad (28)$$

where  $\boldsymbol{\delta}$  is a column vector of incident field components. In particular, for a single incident plane wave in the primary order,  $\boldsymbol{\delta} = [\delta_{p0}]$ . Similarly, from (28) we obtain the solution for the symmetric problem

$$\mathbf{D}^\oplus = -i(\boldsymbol{\sigma}^\oplus + i\mathbf{M})^{-1} \mathbf{J}^\oplus \chi^{-1/2} \boldsymbol{\delta}. \quad (29)$$

Using (15) and (16), the scattering matrix  $\mathcal{S}^\oplus$  for this problem may be inferred from the solution of

$$[\rho_{p0} + \tau_{p0}] = \mathcal{S}^\oplus \boldsymbol{\delta}, \quad (30)$$

by considering all possible incidence configurations. Thus, we derive the scattering matrix

$$\mathcal{S}^\oplus = \mathbf{I} - \frac{2}{D} \chi^{-1/2} \mathbf{K}^{\oplus \mathbf{H}} (\boldsymbol{\sigma}^\oplus + i\mathbf{M})^{-1} \mathbf{J}^\oplus \chi^{-1/2}, \quad (31)$$

where

$$\mathbf{K}^\oplus = \mathbf{U}^\oplus \mathbf{J}^\oplus, \quad \mathbf{U}^\oplus = \text{diag}[\mathbf{U}^{\oplus, \ell}], \quad \mathbf{U}^{\oplus, \ell} = \text{diag}[(-1)^n]. \quad (32)$$

In (31),  $\mathbf{I}$  denotes the identity matrix, and a superscript  $H$  denotes the Hermitian transposition.

The formulation of the antisymmetric problem proceeds along similar lines, and leads to the solution

$$\mathbf{D}^\ominus = i(\boldsymbol{\sigma}^\ominus + i\mathbf{M})^{-1} \mathbf{J}^\ominus \chi^{-1/2} \boldsymbol{\delta}, \quad (33)$$

where  $\mathbf{M}$  is defined in (21), and  $\boldsymbol{\sigma}^\ominus$  and  $\mathbf{J}^\ominus$  are defined as (24) and (26), but with

$$\boldsymbol{\sigma}_{nm}^{\ominus, \ell q} = S_{n-m}^{\ell q} - (-1)^n S_{n+m}^{\ell q}, \quad \mathbf{J}^{\ominus, \ell} = [e^{in\theta_p} - (-1)^n e^{-in\theta_p}] e^{i\alpha_p c \ell}. \quad (34)$$

Thus, for the antisymmetric problem the scattering matrix is

$$\mathcal{S}^\ominus = -\mathbf{I} + \frac{2}{D} \chi^{-1/2} \mathbf{K}^{\ominus H} (\boldsymbol{\sigma}^\ominus + i\mathbf{M})^{-1} \mathbf{J}^\ominus \chi^{-1/2}. \quad (35)$$

Note that for the antisymmetric problem, the coefficients  $C_0^{\ominus, \ell}$  and  $D_0^{\ominus, \ell}$  [see (17) and (18)] vanish identically. Therefore, none of the matrices labelled  $\ominus$  contain the rows and columns corresponding to the cylindrical harmonic  $n = 0$ .

We use the scattering matrices (31) and (35) to define the reflection and transmission matrices,  $\boldsymbol{\rho}$  and  $\boldsymbol{\tau}$ , for a single grating

$$\boldsymbol{\rho} = (\mathcal{S}^\oplus + \mathcal{S}^\ominus)/2, \quad (36)$$

$$\boldsymbol{\tau} = (\mathcal{S}^\oplus - \mathcal{S}^\ominus)/2. \quad (37)$$

Then, for a stack of  $N$  gratings we obtain the amplitude reflection and transmission matrices,  $\boldsymbol{\rho}$  and  $\boldsymbol{\tau}$ , from recurrence relations as detailed in the next section.

### (2c) Recurrence Relations

Using the nomenclature of Fig. 2 we introduce a vector of field components  $\boldsymbol{\delta} = [\delta_p]$ , corresponding to the incident field above the stack (Fig. 2), and vectors of field coefficients  $\mathbf{r} = [r_p]$ , and  $\mathbf{t} = [t_p]$  characterising the reflected and transmitted plane wave field above and below the stack.

The length of the stack evolves by placing a new  $(\nu + 1)^{\text{th}}$  layer, characterised by reflection and transmission scattering matrices  $\boldsymbol{\rho}_{\nu+1}$ ,  $\boldsymbol{\tau}_{\nu+1}$  above a stack of  $\nu$  layers, characterised by the scattering matrices  $\mathcal{R}_\nu$  and  $\mathcal{T}_\nu$ . Note that while an individual layer is up-down symmetric, the stack, in general, does not share this property. Accordingly, while  $\boldsymbol{\rho}_{\nu+1}$  and  $\boldsymbol{\tau}_{\nu+1}$  are the scattering matrices for incidence on a single layer from above or below, we specify that  $\mathcal{R}_\nu$  and  $\mathcal{T}_\nu$  refer to scattering matrices corresponding to the incidence solely from above.

The stack and the incremental layer are separated by a distance  $s$  (Fig. 2), and hence any plane wave propagating across this layer experiences a shift in phase of  $\exp(i\chi_p s)$ . The propagation of a plane wave field  $\mathbf{f}$  can be expressed in the form  $\mathbf{P}\mathbf{f}$  where

$$\mathbf{P} = \text{diag}[e^{i\chi_p s}], \quad \mathbf{f} = [f_p]. \quad (38)$$

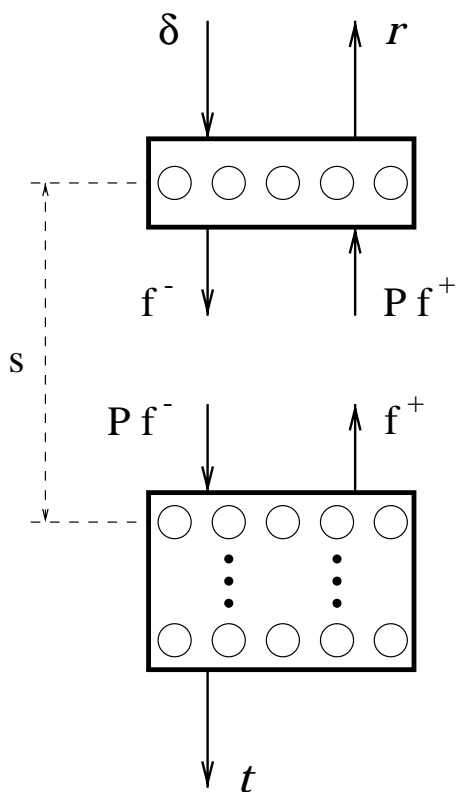


**Fig. 2.** Reflected  $\mathbf{r}$  and transmitted  $\mathbf{t}$  fields, corresponding to an incident field  $\delta$ , normal to a composite stack consisting of two elements.

Between the stack and the layer  $\nu + 1$ , we have an upward going field  $\mathbf{f}^+$  with a phase origin coinciding with the centre of layer  $\nu$ , and a downward propagating field  $\mathbf{f}^-$ , whose phase origin is at the centre of layer  $\nu + 1$ .

The reflected field  $\mathbf{r}$  derives from the reflected component of the incident field  $\rho_{\nu+1}\delta$  and a transmitted component of the upgoing field from below  $\tau_{\nu+1}\mathbf{P}\mathbf{f}^+$ , i.e.

$$\mathbf{r} = \rho_{\nu+1}\delta + \tau_{\nu+1}\mathbf{P}\mathbf{f}^+, \tag{39}$$

and similarly

$$\mathbf{f}^- = \tau_{\nu+1}\delta + \rho_{\nu+1}\mathbf{P}\mathbf{f}^+. \tag{40}$$

The upward propagating field  $\mathbf{f}^+$  derives from a reflection off the stack of the downward propagating field  $\mathbf{P}\mathbf{f}^-$ , while the transmitted field is simply a transmission of  $\mathbf{P}\mathbf{f}^-$  through the stack, i.e.

$$\mathbf{f}^+ = \mathcal{R}_\nu\mathbf{P}\mathbf{f}^-, \tag{41}$$

$$\mathbf{t} = \mathcal{T}_\nu\mathbf{P}\mathbf{f}^-. \tag{42}$$

Solving (39)–(41) we find

$$\mathbf{r} = [\boldsymbol{\rho}_{\nu+1} + \boldsymbol{\tau}_{\nu+1} \mathbf{P} \mathcal{R}_\nu \mathbf{P} (\mathbf{I} - \boldsymbol{\rho}_{\nu+1} \mathbf{P} \mathcal{R}_\nu \mathbf{P})^{-1} \boldsymbol{\tau}_{\nu+1}] \boldsymbol{\delta}, \quad (43)$$

$$\mathbf{t} = [\mathcal{T}_\nu \mathbf{P} (\mathbf{I} - \boldsymbol{\rho}_{\nu+1} \mathbf{P} \mathcal{R}_\nu \mathbf{P})^{-1} \boldsymbol{\tau}_{\nu+1}] \boldsymbol{\delta}, \quad (44)$$

from which the recurrence relations for the reflection and transmission scattering matrices of the stack consisting of  $\nu + 1$  layers may be inferred through

$$\mathbf{r} = \mathcal{R}_{\nu+1} \boldsymbol{\delta}, \quad \mathbf{t} = \mathcal{T}_{\nu+1} \boldsymbol{\delta}. \quad (45)$$

A more compact form of the recurrence relation may be derived by absorbing the propagation terms  $\mathbf{P}$  into the scattering matrices by defining new reflection and transmission scattering matrices

$$\tilde{\mathcal{R}} = \mathbf{P}^{\frac{1}{2}} \mathcal{R} \mathbf{P}^{\frac{1}{2}}, \quad \tilde{\mathcal{T}} = \mathbf{P}^{\frac{1}{2}} \mathcal{T} \mathbf{P}^{\frac{1}{2}}, \quad (46)$$

and similarly for  $\boldsymbol{\rho}$  and  $\boldsymbol{\tau}$ . This has the effect of encapsulating the diffracting element in a symmetric layer of thickness  $s$ , and yields the recurrence relations

$$\tilde{\mathcal{R}}_{\nu+1} = \tilde{\boldsymbol{\rho}}_{\nu+1} + \tilde{\boldsymbol{\tau}}_{\nu+1} \tilde{\mathcal{R}}_\nu (\mathbf{I} - \tilde{\boldsymbol{\rho}}_{\nu+1} \tilde{\mathcal{R}}_\nu)^{-1} \tilde{\boldsymbol{\tau}}_{\nu+1}, \quad \tilde{\mathcal{R}}_0 = \mathbf{0}, \quad (47)$$

$$\tilde{\mathcal{T}}_{\nu+1} = \tilde{\mathcal{T}}_\nu (\mathbf{I} - \tilde{\boldsymbol{\rho}}_{\nu+1} \tilde{\mathcal{R}}_\nu)^{-1} \tilde{\boldsymbol{\tau}}_{\nu+1}, \quad \tilde{\mathcal{T}}_0 = \mathbf{I}. \quad (48)$$

### 3. Numerical Calculations

We have verified the accuracy of our code by comparing the results for a single layer of aluminium cylinders with those obtained by Horwitz *et al.* (1978). We have also checked the reciprocity and the conservation of energy for a simple grating. Another check has been performed in the case of a finite number of layers of dielectric cylinders by comparing our results with those obtained from the code written by Bell *et al.* (1995). In all these cases the numerical results given by our method have been in an excellent agreement with the numerical results produced by the other methods.

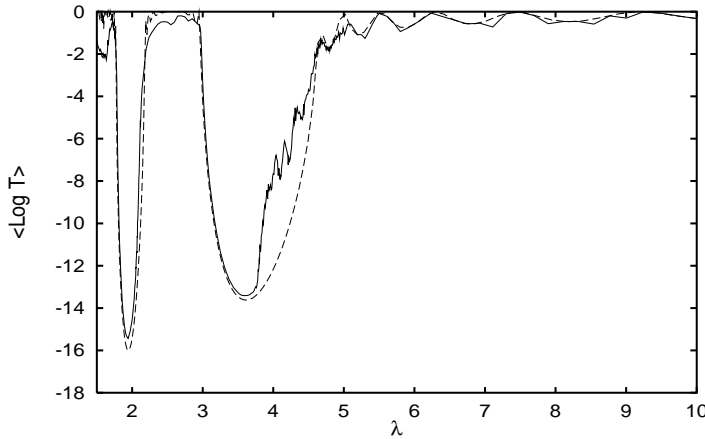


**Fig. 3.** Average of the natural logarithm of transmittance versus wavelength for a stack of ten layers of dielectric cylinders, having the same radius  $a = 0.3 \mu\text{m}$  but a random refractive index uniformly distributed between 2.8 and 3.2, for normal incidence and  $E_z$  polarisation (solid curve). The dashed curve represents the natural logarithm of the transmittance versus wavelength for the same geometry, when the cylinders have the same refractive index  $n = 3.0$ .

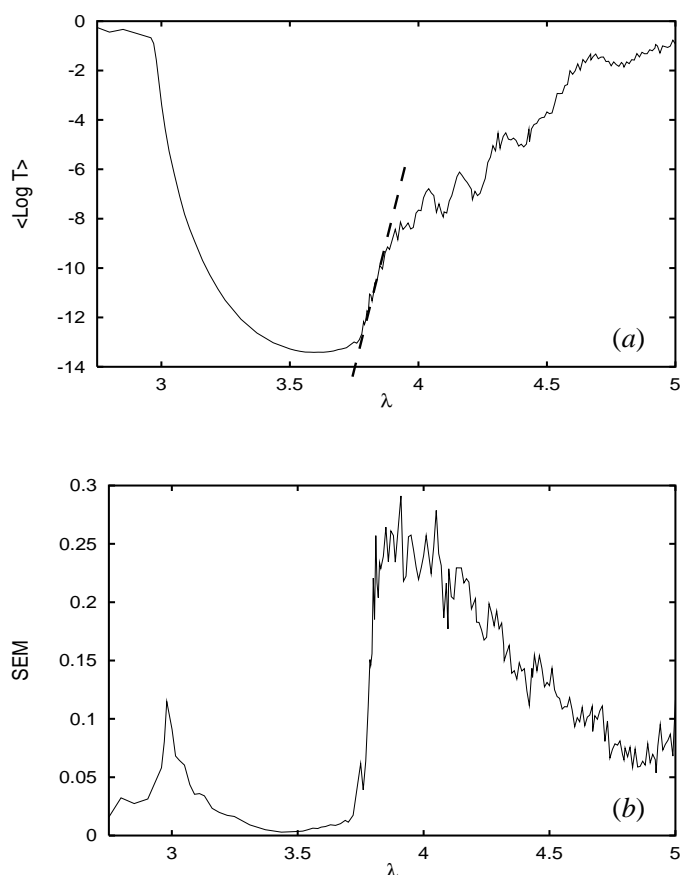


**Fig. 4.** Detail from Fig. 3: (a) region of the band gap with the dashed line marking the Urbach tail with a slope corresponding to a photon energy of 34 eV; (b) standard error in the mean of  $\log T$  versus wavelength.

### (3a) Disordered Dielectric Stacks

We now apply the formulation from the previous section to a particular type of the structure shown in Fig. 1: we consider a stack of dielectric cylinders of radius  $a = 0.3 \mu\text{m}$ , separated by  $d = 1.0 \mu\text{m}$  ( $c = d$ ) in the  $x$ -direction and also by  $s = d$  in the  $y$ -direction. There are 5 cylinders per unit cell so the grating period is  $D = 5.0 \mu\text{m}$ . Each stack consists of 10 gratings. The random element is the refractive indices of the cylinders, which are uniformly distributed between 2.8 and 3.2. Note that the average refractive index 3.0 is sufficiently large to exhibit photonic band gaps for both  $E_z$  and  $H_z$  polarisations (Bell *et al.* 1995; Sigalas *et al.* 1996; McPhedran *et al.* 1997b).

The results of our numerical calculations are presented in Figs 3–6. In Fig. 3 the solid curve represents the averaged natural logarithm of the transmittance as a function of wavelength, for radiation incident along the  $y$ -axis ( $\theta_0 = 0$ ), for  $E_z$  polarisation ( $\mathbf{E}$  parallel to the axes of the cylinders). We choose to display the transmittance logarithmically rather than directly because of its large dynamic

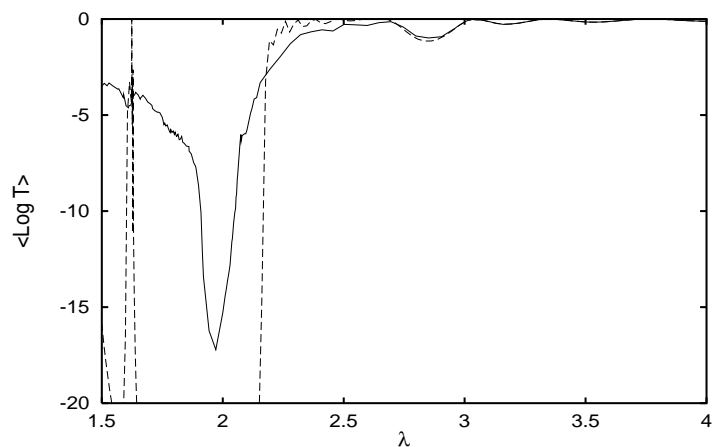


Fig. 5. Same as Fig. 3 but for  $H_z$  polarisation.

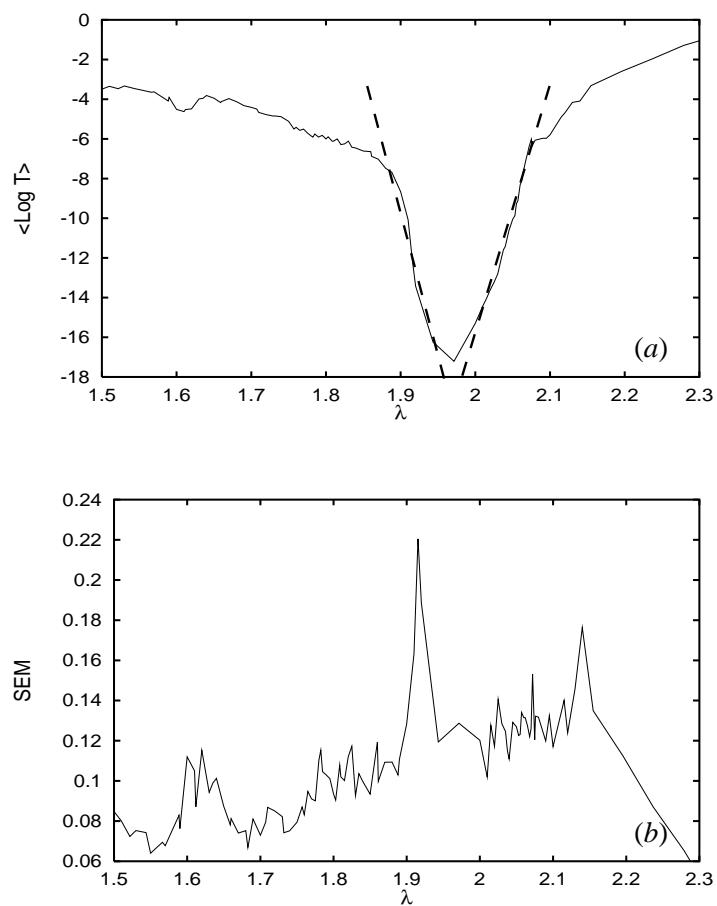


Fig. 6. Detail from Fig. 5: (a) region of the band gap with the dashed lines marking two Urbach tails with slopes corresponding to photon energies of 187 eV (left tail) and 114 eV (right tail); (b) standard error in the mean of  $\log T$  versus wavelength.

range, and also because we are interested in behaviour near the centre of the band gap regions. Each point corresponds to an average over 100 different realisations. The dashed curve in Fig. 3 depicts the natural logarithm of the transmittance for the same structure, but with identical cylinders all having a refractive index  $n = 3.0$ .

The unperturbed structure shows two photonic band gaps, with severely reduced transmittance. The refractive index perturbations have their greatest effect in the lower energy band gap, and interestingly on one side only of this gap. Fig. 4a shows in detail the complicated behaviour of the stack transmittance in this gap. It also indicates (in Fig. 4b) the variation of the standard error in the mean (SEM) of  $\log T$ , in other words the lengths of the ‘error bars’ associated with the points in Fig. 4a. Note that, in fact, the standard error in the mean refers to the sample variability of  $\log T$ , given that  $T$  for each realisation is calculated to an error smaller than 1 part in  $10^5$ . Fig. 4b shows that the transmission on the long-wavelength side of the gap exhibits much larger fluctuations than that on the short-wavelength side. In turn, this suggests differences in the associated electric field distributions. A detailed analysis of this, however, is outside the scope of this paper.

The effect of disorder is to introduce the equivalent of ‘impurity’ levels for electrons (Joannopoulos *et al.* 1995), states with energies within the photonic band gap. An ensemble of such states leads to a distribution of such levels. In analogy to solid state physics, we refer to these as Urbach (1953) tails if they occur near the centre of a gap (along the dashed line in Fig. 4a), and Tauc (1974) tails nearer the gap edges. We can see in Fig. 4b two clear regions, one where the SEM increases rapidly, while in the second fluctuations are superimposed on a slow decrease.

The Urbach tail in Fig. 4a has a slope corresponding to a photon energy of 3.4 eV. This is deduced by assuming a dependence on the wavelength of the form

$$\frac{1}{Nd} \langle \log T \rangle \sim e^{-\lambda/\lambda_0}, \quad (49)$$

and using a least-squares fit in the region of the Urbach tail we obtain  $\lambda_0 = 0.368 \mu\text{m}$ . In contrast with results from studies of optical properties of amorphous semiconductors, these parameters are not universal. Another difference arises from the fact that in the case of amorphous semiconductors we have positional disorder of the scattering centres, while in our simulations the cylinders form a two-dimensional crystal, and it is the refractive index which varies. Also, in an amorphous semiconductor, in the region of an Urbach tail we have weak scattering of electrons, while in a photonic crystal the photons are scattered strongly. Finally, differences may appear because our results correspond to the solution of a two-dimensional problem, and the study of amorphous semiconductors involves the solution of a three-dimensional problem.

In Fig. 5 we show the variation of  $\log T$  with wavelength for the same structure as in Fig. 3, but with an incident radiation  $H_z$  polarised ( $\mathbf{H}$  parallel to the axes of the cylinders). Also, Fig. 6a represents the region of the second lowest energy gap in Fig. 5, enlarged, while Fig. 6b displays the SEM of  $\log T$  in the same

region. The number of layers would have to be increased to around 25 for the lowest energy gap to be well-developed with this polarisation.

For  $H_z$  polarisation, the second gap is greatly weakened by the refractive index variation. Both sides of the gap appear to have developed almost symmetric Urbach tails (Fig. 6a), but the correlation of these with the behaviour of the SEM (Fig. 6b) is less clear than in Fig. 4. In this case the slopes of the Urbach tails correspond to energies of 15.8 eV (left tail) and 8.5 eV (right tail), corresponding to  $\lambda_0 = 0.079$  and  $0.146 \mu\text{m}$ , respectively.

The differences with respect to the  $E_z$  polarisation are evident and they can be explained by the differences in the effective dielectric constants for the two polarisations. Thus, in the case of  $E_z$  polarisation, the effective dielectric constant of the array is

$$\varepsilon_E^* = \frac{\pi a^2}{d^2} \sum_{q=1}^{N_c} \varepsilon_q + N_c \left( 1 - \frac{\pi a^2}{d^2} \right), \quad (50)$$

by analogy with the behaviour of capacitors in parallel, while for  $H_z$  polarisation the effective dielectric constant of the array is determined by the dipole coefficients  $\{B_1^1, \dots, B_1^q\}$  from equation (12), corresponding to capacitors in series.

### (3b) Periodic Metallic Stacks

Here, we discuss a second case, where the stack consists of metallic cylinders having a complex refractive index. Hence, we allow cylinders to have absorption. We concentrate on the structure with all the cylinders having the same radius and the same refractive index ( $n = n' + in''$ ). Also, the distances between the centres of successive cylinders ( $d$ ) are equal to each other, and to the distances between successive layers ( $s = d$  in Fig. 1). Accordingly, the stack of gratings is a slice from a square array of identical cylinders parallel to the  $z$ -axis.

In this case we can take a single cylinder per unit cell (a square of size  $d$ ) and the Rayleigh identity for a single layer reduces to

$$iM_\ell B_\ell + \sum_{m=-\infty}^{\infty} S_{\ell-m} B_m = -i(-1)^\ell e^{-i\ell\theta_0} \chi_0^{-1/2}. \quad (51)$$

Also, in terms of the  $B$  coefficients, the amplitude reflection and transmission coefficients (15) and (16) become

$$\rho_{p0} = \frac{2}{id} \chi_p^{-1/2} \sum_{m=-\infty}^{\infty} e^{-im\theta_p} B_m, \quad (52)$$

$$\tau_{p0} = \delta_{p0} + \frac{2}{id} \chi_p^{-1/2} \sum_{m=-\infty}^{\infty} (-)^m e^{im\theta_p} B_m. \quad (53)$$

Now the coefficients  $M_\ell$  in (51) are complex and we have the absorptance due to a single layer given by the formula

$$A' = -\frac{4}{\chi_0 d} \sum_{m=-\infty}^{\infty} |B_m|^2 \operatorname{Im}(M_m), \quad (54)$$

and the conservation of energy in the form

$$\sum_{p \in \Omega} \left[ |\rho_{p0}|^2 + |\tau_{p0}|^2 \right] + A' = 1. \quad (55)$$

The scattering matrices (31) and (35) can be used here as well, but with the matrices adapted to the case of a single cylinder inside the unit cell ( $N_c = 1$ ).

For a stack of  $N$  layers, we use the recurrence relations (47) and (48) to obtain the total reflection and transmission amplitudes for the stack. Then, we employ (45) to evaluate the total reflectance and transmittance

$$\mathcal{E}_R = \sum_{p \in \Omega} |r_p|^2, \quad (56)$$

$$\mathcal{E}_T = \sum_{p \in \Omega} |t_p|^2. \quad (57)$$

Finally, the total absorptance of the  $N$ -layer stack is obtained from the conservation of energy

$$A = 1 - \mathcal{E}_R - \mathcal{E}_T. \quad (58)$$

For numerical calculations we consider a stack of 25 gratings, each grating being a one-dimensional array of gold rods of radius  $a = 0.2 \mu\text{m}$ . The period of the grating is  $d = 1 \mu\text{m}$  and the distance between gratings  $h = d$ . The refractive index for gold, as a function of wavelength, was obtained by interpolating the comprehensive data set compiled by Palik (1993) (see Fig. 7). We have also used an extrapolation method based on reflectance data for wavelengths between  $\lambda = 10$  and  $20 \mu\text{m}$ . The reflectance, transmittance and absorptance, versus the wavelength, for normal incidence and  $E_z$  polarisation ( $V = E_z$ ) are shown in the right panel of Fig. 8.

In the left panel of Fig. 8 we show the dispersion curves for a square array of perfectly conducting cylinders with the same radius and period as the gold rods. The crystal momentum  $\mathbf{k}_0$  is along the  $x$ -axis. The dispersion curves show the cutoff frequency between  $k_\perp = 0$  and the minimum of the first photonic band, which appears when we solve the Dirichlet problem for this structure (Nicolrovici *et al.* 1995).

By comparing the two panels we can see that, in the region of cutoff frequency ( $\lambda \gtrsim 2.0 \mu\text{m}$ ), the transmittance of the stack is extremely small (actually we have obtained numerical values of the order  $10^{-100}$ ), the absorption is not too high and tends to zero as the wavelength increases and the reflectance tends

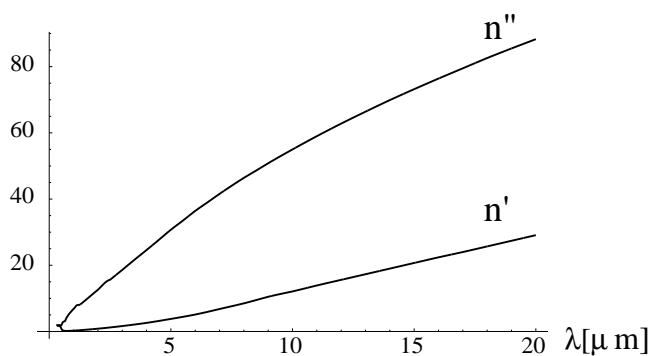


**Fig. 7.** Refractive index ( $n = n' + in''$ ) for gold as a function of wavelength, obtained by interpolation of data compiled by Palik (1993), together with an extrapolation based on reflectance data between 10 and 20  $\mu\text{m}$ .

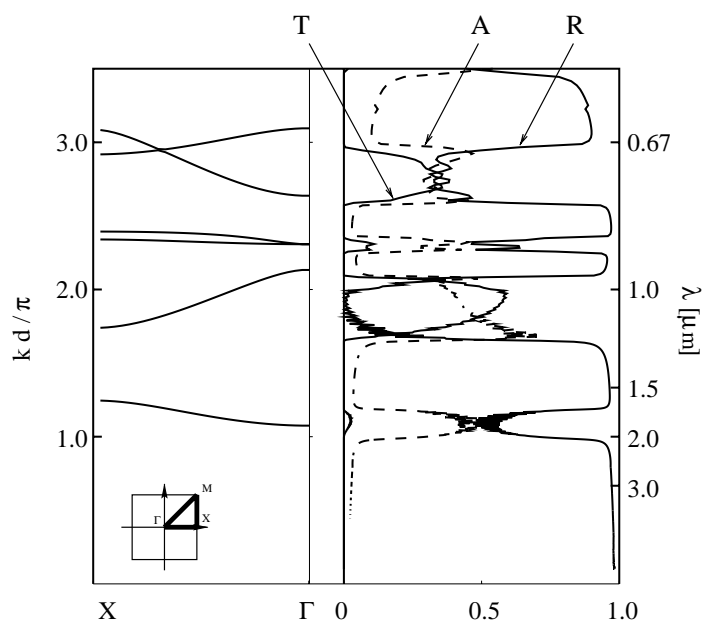


**Fig. 8.** *Left panel:* photonic band diagram for  $E_z$  polarisation for a square array of perfectly conducting cylinders, with  $a = 0.20 \mu\text{m}$  and  $d = 1.0 \mu\text{m}$ . *Right panel:* reflectance R, transmittance T and absorptance A for a stack of 25 equidistant gratings of gold cylinders, of the same radius  $a$ , for normal incidence and  $E_z$  polarisation. The distance between layers is  $d$ . The inset shows the irreducible octant in the first Brillouin zone for a square array.

to 1. Note that this comparison is allowed because the rods of gold are highly conducting at long wavelengths.

In the region of the lowest photonic band the reflectance is almost 50% and this decrease is accompanied by a high absorptance, while the transmittance remains low. When the radius of the cylinders in the array varies, the minimum of the lowest photonic band (located at  $\Gamma$  in Fig. 8) is given by the formula (Nicorovici *et al.* 1995; Guida *et al.* 1998)

$$k_{\min} = \left[ -\frac{d^2}{2\pi} \ln \left( \frac{2a}{d} \right) + \text{constant} \right]^{-1/2}. \quad (59)$$

Thus, when the radius of the gold rods decreases the region of enhanced absorption widens and moves to the region where the bulk gold strongly reflects. This remarkable effect is completely different from the case of dielectric inclusions, where there is no absorptance and the reflectance is reduced by a high transmittance. Similar results have been obtained for other metals such as aluminium layers, with  $s = d$  in Fig. 1.

The same behaviour arises if we consider a semi-infinite array of gold rods in the region  $y < 0$ . For  $\lambda > d$ , we then have only one propagating order, and all the quantities in (47) and (48) are scalars. Thus, by denoting

$$\lim_{N \rightarrow \infty} \tilde{\mathcal{R}}_N = \tilde{\mathcal{R}}_\infty \quad (60)$$

in (47), we obtain the fixed point formula

$$\tilde{\mathcal{R}}_\infty = \tilde{\mathcal{R}} + \tilde{\mathcal{T}} \tilde{\mathcal{R}}_\infty \left( 1 - \tilde{\mathcal{R}} \tilde{\mathcal{R}}_\infty \right)^{-1} \tilde{\mathcal{T}}, \quad (61)$$

with the solution

$$\tilde{\mathcal{R}}_\infty = \frac{1 - \tilde{\mathcal{R}}^2 - \tilde{\mathcal{T}}^2 \pm \sqrt{\left( 1 - \tilde{\mathcal{R}}^2 - \tilde{\mathcal{T}}^2 \right)^2 - 4\tilde{\mathcal{R}}^2}}{2\tilde{\mathcal{R}}}, \quad (62)$$

where the root of minimum modulus is chosen. In this case the reflectance of the array is given by  $\mathcal{E}_R^\infty = |\tilde{\mathcal{R}}_\infty|^2$  and we can see in Fig. 9 that the dashed line representing  $\tilde{\mathcal{R}}_\infty$  follows the average of the total reflectance of the finite array.

The transmittance of the semi-infinite array has the form

$$\mathcal{E}_T^\infty = \lim_{N \rightarrow \infty} \left| \tilde{\mathcal{T}}_N \right|^2, \quad (63)$$

and from (48) we can only approximate

$$\tilde{\mathcal{T}}_N \simeq \tilde{\mathcal{T}} \left( \frac{\tilde{\mathcal{T}}}{1 - \tilde{\mathcal{R}} \tilde{\mathcal{R}}_\infty} \right)^{N-1} \rightarrow 0 \quad \text{as } N \rightarrow \infty. \quad (64)$$

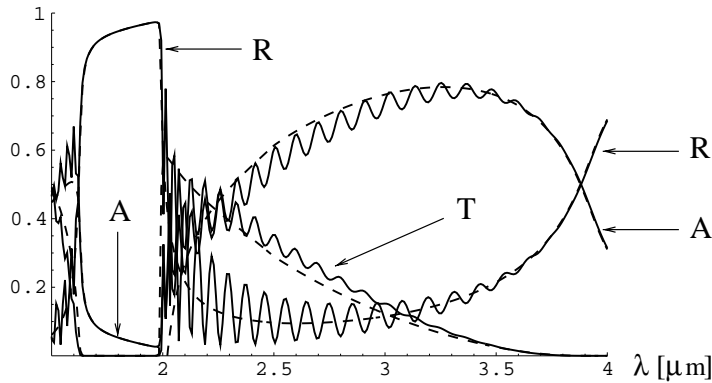


**Fig. 9.** Reflectance  $R$ , transmittance  $T$  and absorptance  $A$  for a stack of 25 equidistant gratings of gold cylinders of radius  $a = 0.05 \mu\text{m}$ , for normal incidence and  $E_z$  polarisation. The distance between cylinders and between gratings is  $d = 1.0 \mu\text{m}$ . The dashed lines represent the results from the fixed point formulas (62), (64) and (65).

Hence, the transmittance of the semi-infinite array tends to zero as expected in the presence of absorption. Finally, the absorptance is given by

$$A_\infty \simeq 1 - \mathcal{E}_R^\infty. \quad (65)$$

We can see in Fig. 9 that, for relatively short wavelengths, the transmittance is underestimated due to the approximations used to obtain (64), while the absorptance is overestimated, but the differences are negligible for long wavelengths. A detailed discussion of these results will be given elsewhere.

#### 4. Conclusions

We have developed a novel method which allows us to investigate stacks of gratings, consisting of circular cylinders. We have described some of the first applications of the method to stacks of metallic simple gratings, and to stacks of layers in which only the refractive index of the cylinders varied randomly. In future work we will investigate the cases when the cylinder radius and positions vary randomly, as well as the case when the distance between successive layers is random.

Our method can be generalised to coated cylinders. Also, it can be used to study crossed stacks with rotation of layers (one layer to the next), by using rotation matrices (Botten *et al.* 1997) in the argument which treats the derivation of the recurrence relations coupling layers together. A particular choice of crossing angle of  $0^\circ$  and  $90^\circ$  produces polarisation insensitivity.

#### Acknowledgments

The Australian Research Council supported this work. Some of the numerical results presented here were obtained on a Parallel Virtual Machine computer cluster which was established with support from ARC RIEF funds. Helpful discussions with D. R. McKenzie are acknowledged.

## References

- Abramowitz, M., and Stegun, I. A. (1972). 'Handbook of Mathematical Functions', p. 363 (Dover: New York).
- Bell, P. M., Pendry, J. B., Moreno, L. M., and Ward, A. J. (1995). *Comput. Phys. Commun.* **85**, 306.
- Botten, L. C., McPhedran, R. C., Nicorovici, N. A., and Derrick, G. H. (1997). *Phys. Rev. B* **55**, 16072.
- Dowling, J., Everitt, H., and Yablonovitch, E. (1998). 'Photonic & Acoustic Band-gap Bibliography', <http://home.earthlink.net/~jpdowling/pbgbib.html>.
- Felbacq, D., Tayeb, G., and Maystre, D. (1994). *J. Opt. Soc. Am. A* **11**, 2526.
- Guida, G., Maystre, D., Tayeb, G., and Vincent, P. (1998). *J. Opt. Soc. Am. B* **15**, 2308.
- Ho, K. M., Chan, C. T., and Soukoulis, C. M. (1990). *Phys. Rev. Lett.* **65**, 3152.
- Horwitz, C. M., McPhedran, R. C., and Beunen, J. (1978). *J. Opt. Soc. Am.* **68**, 1023.
- Joannopoulos, J. D., Meade, R. D., and Winn, J. N. (1995). 'Photonic Crystals: Molding the Flow of Light' (Princeton Univ. Press: New Jersey).
- Leung, K. M., and Liu, Y. F. (1990). *Phys. Rev. Lett.* **65**, 2646.
- Li, L.-M., and Zhang, Z.-Q. (1998). *Phys. Rev. B* **58**, 9587.
- Lo, K. M., McPhedran, R. C., Bassett, I. M., and Milton, G. W. (1994). *IEEE J. Lightwave Technol.* **12**, 396.
- McPhedran, R. C., Nicorovici, N. A., Botten, L. C., and Bao Ke-Da (1997a). In 'IMA Volumes in Mathematics and its Applications', Vol. 96 (Ed. G. Papanicolau), p. 155 (Springer: New York).
- McPhedran, R. C., Nicorovici, N. A., and Botten, L. C. (1997b). *J. Electromagn. Waves Applic.* **11**, 981.
- Nicorovici, N. A., and McPhedran, R. C. (1994). *Phys. Rev. E* **50**, 3143.
- Nicorovici, N. A., McPhedran, R. C., and Botten, L. C. (1995). *Phys. Rev. E* **52**, 1135.
- Palik, E. D. (1993). 'The Handbook of Optical Constants of Solids' (Academic: New York).
- Pendry, J. B., and MacKinnon, A. (1992). *Phys. Rev. Lett.* **69**, 2772.
- Sigalas, M. M., Soukoulis, C. M., Chan, C.-T., and Turner, D. (1996). *Phys. Rev. B* **53**, 8340.
- Soukoulis, C. M. (1993). 'Photonic Band Gaps and Localization' (Plenum: New York).
- Tauc, J. (1974). In 'Amorphous and Liquid Semiconductors' (Ed. J. Tauc), p. 159 (Plenum: London).
- Twersky, V. (1961). *Arch. Rational Mech. Anal.* **8**, 323.
- Urbach, F. (1953). *Phys. Rev.* **92**, 1324.
- von Ignatowsky, W. (1914). *Ann. Physik (Leipzig)* **44**, 369.
- Wijnngaard, W. (1973). *J. Opt. Soc. Am.* **63**, 944.